PRAMANA
— journal of
physics

Vol. 70, No. 1
January 2008
pp. 61–73

Energy and intensity distributions of 279 keV multiply scattered photons in bronze – an inverse response matrix approach

MANPREET SINGH, BHAJAN SINGH and B S SANDHU*
Physics Department, Punjabi University, Patiala 147 002, India
*Corresponding author. E-mail: balvir@pbi.ac.in; balvir99@indiatimes.com

MS received 22 February 2007; revised 13 July 2007; accepted 7 August 2007

Abstract. An inverse response matrix converts the observed pulse-height distribution of a NaI(Tl) scintillation detector to a true photon spectrum. This also results in extraction of intensity and energy distributions of multiply scattered events originating from interactions of 279 keV photons with thick targets of bronze. The observed pulse-height distributions are a composite of singly and multiply scattered events in addition to bremmstrahlung originating from slowing down of Compton and photo-electrons in thick targets. To evaluate the contribution of multiply scattered events, the spectrum of singly scattered events contributing to inelastic Compton peak is reconstructed analytically. The optimum thickness (saturation depth), at which the number of multiply scattered events saturate, has been evaluated in different energy bin meshes chosen for scintillation detector response unfolding. Monte Carlo calculations based upon the package developed by Bauer and Pattison (Compton scattering experiments at the HMI (1981), HMI-B 364, pp. 1–106) supports the present experimental results.

Keywords. Multiple Compton scattering; scintillation detector response unfolding; energy and intensity distributions; saturation thickness.

PACS Nos 13.60.-Fz; 32.80.-Cy; 78.70.-g

1. Introduction

One of the unresolved problems in experimental Compton scattering measurements is the extent to which the accuracy of measured Compton profiles is affected by events in which the incident photon is scattered more than once. Because of the low Compton cross-sections (≈0.5 barns per atom), samples of several mm thicknesses need to be included in the measurements to obtain reasonable intensity of Compton scattered photons. In such experimental conditions involving thick targets, the incident photon undergoes a number of scattering and collisions within the sample before coming out of it. These multiple scatterings of photons act as a background in Compton scattering measurements and errors up to 10% of the peak-height of the profiles may get introduced if the contribution due to multiply scattered events is neglected. The energy distribution in the multiply scattered spectrum

is broader than for singly scattered line shapes. The unique relationship between photon energy and electron momentum is also lost resulting in incorrect evaluation of Compton profiles.

For correct evaluation of Compton profiles, the multiple scattering has been investigated both experimentally and theoretically using analytical and Monte Carlo methods. Because of the large number of experimental parameters that must be followed by Monte Carlo simulations, these become both unwieldy and time consuming, in addition to the unavoidable increase in statistical errors that follow this type of correction procedure. Thus it becomes difficult to assess the accuracy and reliability of an individual corrected Compton profile.

Halonen and Williams [1] have performed measurements to correct the data of Compton profiles from multiple scattering contaminations in the pure samples of Al and Ni in the backward hemisphere for incident photon energies of 60 and 159 keV. The experimental measurements of multiple scattering, at 662 keV gamma photon energy, have investigated the effect of target thickness [2], exact electron momentum distribution in an atom [3,4] and effect of detector collimator and sample thickness [5] on multiple scatterings from the pure samples. Barnea *et al* [6] have investigated multiply scattered fraction (MSF) in samples of brass (alloy) and tin, and concluded that MSF first increases and then saturates with increase in energy window width around the centroid of inelastic scattered peak. Our measurements [7] provide the experimental observation of Z-dependence of saturation depth of 662 keV multiply scattered gamma rays. The scattered photon flux is detected by an HPGe detector placed at right angle to the incident beam. The measurements have confirmed that saturation depth (in cm) decreases with increasing atomic number of the target. The intensity of observed doubly scattered peak is also found to be decreasing with increasing Z-number. More recently, our measurements [8] provide useful information about multiple scattering of 0.279-, 0.662- and 1.12-MeV gamma photons from thick targets of copper at 60° scattering angle. These measurements have confirmed that the saturation depth increases with increase in incident photon energy, the signal-to-noise ratio decreases with increasing target thickness and MSF increases and saturates with an increase in energy window around the Compton scattered peak.

The available data on multiple scattering [8] of 279 keV incident photons are confined to copper target at scattering angle of 60° only. Also no attempt has been made so far to evaluate the contribution of multiply scattered photons in energy regions other than the photo-peak. In this paper we have presented an inverse matrix approach which first converts the observed pulse-height distribution to a photon spectrum (response function of the scintillation detector) and then helps in the extraction of the multiply scattered events in different energy bin meshes, chosen for scintillation detector response unfolding, from the targets of bronze of varying thickness.

2. Experimental set-up

The experimental arrangement used for the present measurements is shown in figure 1. A well-shielded and collimated radioactive source of ^{203}Hg of strength 25 mCi provides a narrow beam of 279 keV gamma rays. The rectangular samples of bronze

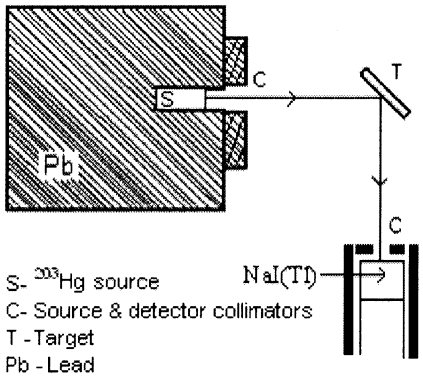

Figure 1. Experimental arrangement (dimensions not scaled) for present measurements.

of dimensions 80 mm in length and 40 mm in breadth (thickness varying from 1 mm to 25 mm) are placed at a distance of 152 mm from the source collimator so that the angular spread due to the source collimator (radius 6 mm) on the bronze target is limited to $\pm 2.3°$.

The collimated beam of 279 keV gamma rays is incident obliquely at an angle of 45° and the scattered beam is also detected obliquely at a reflecting angle of 45°, so that the incident and scattered beams are 90° apart. The radiations scattered from the target are detected by a properly shielded NaI(Tl) scintillation detector having dimensions 51 × 51 mm placed 90° to the incident beam. The field of view of the NaI(Tl) detector is confined to the irradiated sample only. In multiple scattering experiments, the energy resolution of the detector is of secondary importance compared to efficiency because of low values of intensity to be measured. So NaI(Tl) detector is preferred for intensity measurements in comparison to semiconductor detectors. Also the scattering angle of 90° has been chosen especially because in choosing small scattering angle there will be considerable coherent distribution in the recorded scattered spectrum. At large scattering angles, the scattered photon flux decreases, resulting in poor counting statistics. A compromise is therefore made in choosing a scattering angle of 90° to estimate the energy and intensity distributions of multiply scattered radiation.

The assembly of source-collimator, target, gamma ray detector and detector-collimator are placed in such a way that their common axes passes through the centre of the target. The distance between the front face of the target and the detector-collimator (radius 6 mm) is kept at 92 mm, so that the angular spread about the median ray in the direction of the gamma detector is $\pm 3.7°$. The scintillation detector is properly shielded by a cylindrical lead shielding having the inner side covered with 2 mm thick iron and 1 mm thick aluminium, with iron facing lead to absorb K X-rays emitted by lead shielding. The angular aperture due to source collimator is too small, so the photons scattered from the source collimator followed by another scattering from the target have energy approximately equal to the singly scattered energy. Owing to the radius of the cylindrical lead shielding of the gamma detector, the singly scattered photons from the target followed by

another scattering from the detector shielding have energy lower than corresponding to observed inelastic scattered peak's energy.

3. Method of measurements

The principle of the present measurements is based on the detection of the scattered photon flux from the bronze targets of various thicknesses by placing a properly shielded NaI(Tl) scintillation detector at the desired angular position relative to the primary gamma beam. The experiment is designed to detect all the scattered photons from the bronze targets at 90°. The experimental data are accumulated on a PC-based ORTEC Mastreo-32 Multi channel analyzer (MCA). The measuring time for each thickness of the sample is 10 ks with the background also recorded for the same time duration. To evaluate the true scattered spectrum for each thickness, the spectra are taken with and without the sample in the primary incident beam. In order to determine the contribution due to multiply scattered photons only, the spectrum of singly scattered photons is reconstructed analytically, which is described in detail in our recent work [8]. The subtraction of this reconstructed normalized singly scattered spectrum from the observed experimental spectrum gives the number of multiply scattered photons under the full energy peak. However to take into account the contribution due to low pulse-height counts resulting from the partial absorption of higher energy photons, we make use of an inverse matrix approach [8–10], which shifts these low pulse-height counts into their photo-peak energy region by unscrambling the pulse-height distributions recorded by NaI(Tl) gamma ray detector.

4. Inverse response matrix formation

In the observed spectra, the pulses resulting from the partially absorbed photons get superimposed on the true photon spectra. Increasingly complex and sophisticated methods are being used for the conversion of observed NaI(Tl) pulse-height distributions in to gamma ray spectra. We have performed this conversion of pulse-height distributions of the NaI(Tl) crystal (consisting of a peak and a continuous distribution of pulses) to a true photon energy spectrum with the help of a response matrix approach [8–10]. Since FWHM of the photo-peak varies as $E_o^{1/2}$, where E_o is the incident source energy, the $E^{1/2}$ scale is chosen to make the photo-peaks of constant width. In the present measurement a bin mesh ($E^{1/2}$) is chosen to be 0.05 $(\text{MeV})^{1/2}$, instead of 0.1 $(\text{MeV})^{1/2}$ used in our early measurements [8] and by Hubbell *et al* [9,10], to achieve better accuracy. Therefore a 12×12 matrix is constructed to cover an energy range from $E^{1/2} = 0.05$ to 0.6 $(\text{MeV})^{1/2}$, or $E = 2.5$ to 360 keV. The pulse-height distributions for energies 279, 511, 662 and 834 keV are obtained experimentally from mono energetic sources by placing each of the sources at the irradiating target's position in the present experimental geometry. After normalizing the areas under their respective photo-peaks to intrinsic (crystal) efficiency values, these distributions are then smoothed so as to include the peaks (figure 2a) resulting only from the interactions after the entry of photons

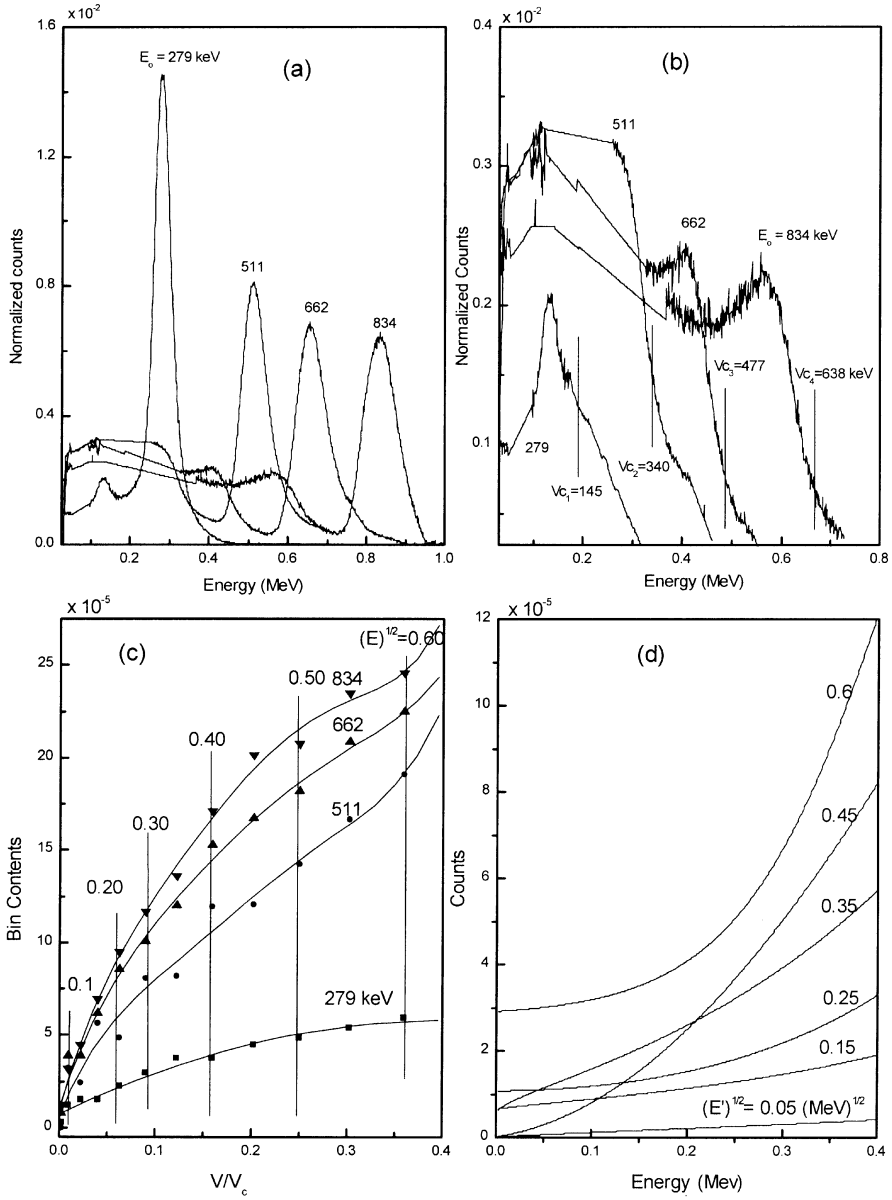

Figure 2. (**a**) Available pulse-height distributions from mono-energetic sources, areas normalized to crystal efficiency; (**b**) photo-peaks of the curves of figure 2a have been subtracted off and the theoretical Compton edges, V_c, noted; (**c**) transformation to V/V_c scale, cross cuts of constant V/V_c are indicated and (**d**) interpolated bin content counts vs. incident energy at different values of $(E')^{1/2}$.

into the crystal. The intrinsic (crystal) efficiency values [11] are calculated using the theoretical attenuation coefficients for NaI[Tl] and the thickness of the detector.

After omitting the photo-peaks of these smoothed curves and marking their theoretical Compton edges (V_{c1}, V_{c2}, V_{c3} and V_{c4}) (figure 2b), all of these four different distributions for different source energies are plotted linearly on V/V_c scale (figure 2c), where V_c is the theoretical Compton edge for each energy.

Each distribution is then divided into energy bins of constant width in terms of $(E)^{1/2}$ MeV. Labelling each bin by its top energy, the bin content distributions for the given source energies E_o, are plotted as a function of $(E')^{1/2}$. Then after the interpolation of these curves, a series of curves for each of the bin ranging from $(0.1)^{1/2}$ MeV to $(1.0)^{1/2}$ MeV are obtained in the energy range from 0 to 1 MeV as shown in figure 2d. The curves having different $(E')^{1/2}$ values (figure 2d) are then further divided into energy bins of width equal in $E^{1/2}$ MeV and the bin contents are written in the form of a triangular matrix (**R**) having elements R_{ij}, where the indices i and j refers to incident energy E and pulse-height of each energy bin E'. The sum of each row is equated to $\{1 - \varepsilon_p(E)\varepsilon_i(E)\}$, where $\varepsilon_i(E)$ is the intrinsic (crystal) efficiency of the scintillation detector already calculated and $\varepsilon_p(E)$ is the peak-to-total ratio [11] for the scintillation detector at energy E. The photo-peak (full energy peak) efficiency $\varepsilon_i(E)\varepsilon_p(E)$ is then added to the principal diagonal of the matrix, making each row equal to $\varepsilon_i(E)$. For each ith energy, a summation over all j values equals to the crystal efficiency, the resultant matrix (table 1) with elements R_{ij} is a desired response matrix, which converts the photon spectra $N(E)$ into expected measured pulse-height distribution $S(E')$ as

$$S_j = \sum_{i=1}^{N} N_i R_{ij}, \tag{1}$$

where S_j and N_i are formed from $S(E')$ and $N(E)$ in a manner similar to R_{ij}. Therefore if we have to obtain original spectra from the measured pulse-height distribution, then the above response matrix (**R**) is to be inverted. A FORTRAN program [12] does this inversion. The response of the scintillation detector used in present experiment to record the observed pulse-height distribution is obtained by simple matrix multiplication of $S(E')$ and R_{ij}^{-1} as

$$N_i = \sum_{j=1}^{N} S_j R_{ij}^{-1}. \tag{2}$$

Therefore the response of the detector (table 2) is given by number of photons per energy bin as

$$N(E) = \frac{N_i}{E_i - E_{i-1}}, \tag{3}$$

where $N(E)$ is in units of photons per unit energy interval and is the response-corrected spectrum.

Table 1. Response matrix, **R**, with elements R_{ij}, of the NaI(Tl) detector. The $E^{1/2}$ values refer to tops of energy bins. Each row corresponds to a pulse-height distribution due to line source of energy $E - \Delta E/2$ normalized to the efficiency of the crystal. 10^{-3} should multiply the numbers.

	$(E')^{1/2}$											
$(E)^{1/2}$	0.05	0.10	0.15	0.20	0.25	0.30	0.35	0.40	0.45	0.50	0.55	0.60
0.05	1000											
0.10	2	998										
0.15	0	1	998									
0.20	1	2	17	980								
0.25	1	2	12	2	982							
0.30	2	4	16	4	22	952						
0.35	2	5	14	5	18	7	950					
0.40	2	7	14	8	18	12	28	911				
0.45	2	8	13	11	17	16	28	18	885			
0.50	2	8	11	12	15	18	26	22	28	836		
0.55	2	8	9	13	13	19	23	24	28	31	775	
0.60	2	8	7	13	11	19	20	25	27	32	36	700

Table 2. Inverted response matrix, $\mathbf{R}^{-1}$, with elements R_{ij}, in the same units as table 1. 10^{-3} should multiply the numbers.

	$(E')^{1/2}$											
$(E)^{1/2}$	0.05	0.10	0.15	0.20	0.25	0.30	0.35	0.40	0.45	0.50	0.55	0.60
0.05	1000											
0.10	−2	1002										
0.15	−0	−0	1002									
0.20	−1	−2	−17	1020								
0.25	−1	−2	−12	−2	1018							
0.30	−2	−4	−16	−4	−24	1050						
0.35	−2	−5	−14	−5	−19	−8	1053					
0.40	−2	−8	−14	−9	−19	−14	−32	1098				
0.45	−2	−8	−13	−12	−18	−18	−33	−22	1130			
0.50	−2	−9	−11	−14	−16	−21	−31	−28	−38	1196		
0.55	−2	−9	−9	−16	−14	−24	−28	−32	−39	−48	1290	
0.60	−2	−10	−7	−16	−12	−25	−25	−35	−40	−52	−66	1429

5. Results and discussion

Curve a in figure 3 shows a typical observed spectrum of bronze for 10 ks. The spectrum is stripped for the inelastic peak resulting from interactions of 74 keV (line of ^{203}Hg-source) and the background is also subtracted. The observed pulse-height distributions are a composite of singly as well as multiply scattered photons along with bremsstrahlung events. The singly scattered events under the full energy peak

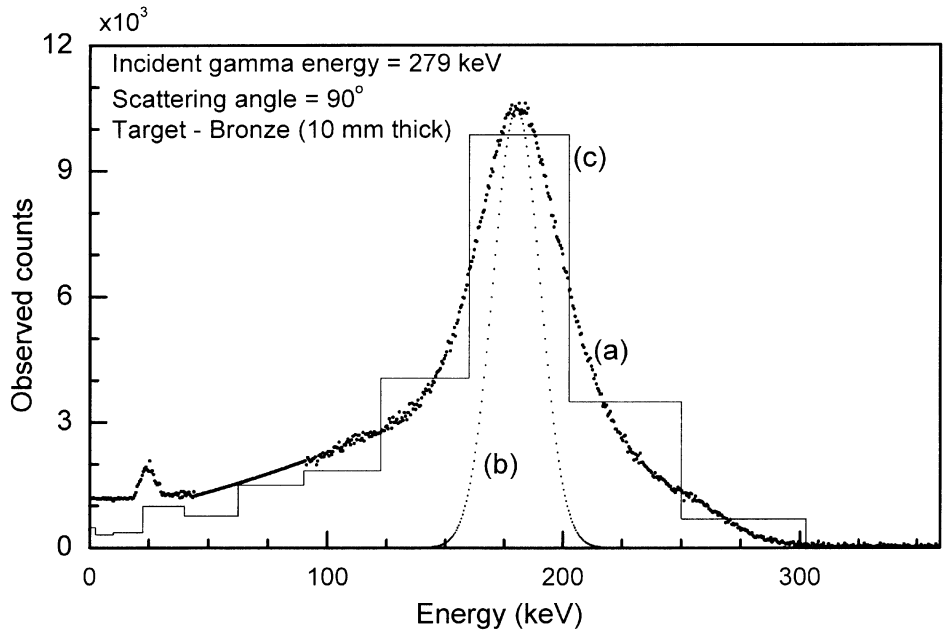

Figure 3. Experimentally observed pulse-height distributions, $S(E')$ (Curve a) obtained after stripping off the inelastic peak resulting from interactions of 74 keV X-rays and subtracting background events of 279 keV incident photons with bronze target of 10 mm thickness at scattering angle of 90° for 10 ks irradiation time. Normalized analytically reconstructed singly scattered full energy peak (Curve b) and resulting calculated histogram (Curve c) of $N(E)$ converting pulse-height distribution to a true photon spectrum.

[8] are obtained by reconstructing analytically the singly scattered inelastic peak using the experimentally determined parameters, such as FWHM and the detector efficiency of the detector corresponding to the singly scattered energy, counts under the photo-peak and the Gaussian distribution of inelastically scattered peak. The analytically reconstructed singly scattered peak is shown by curve b in figure 3.

The experimental pulse-height distribution, $S(E')$, (Curve a) is converted to a photon energy spectrum with the help of the inverse response matrix (given in §4 above). The solid Curve c is the resulting calculated histogram of $N(E)$ in units of photons, also known as the response function of the scintillation detector. Low pulse-height counts resulting from partial absorption of higher energy photons are shifted to the photo-peak energy region. The events under the histogram in the Compton continuum accounts for photons of reduced energy (less than that of inelastically Compton scattered peak) originating from multiple interactions in the target and bremsstrahlung events, and finally escaping in the direction of the gamma detector. Since the full-energy peak does not fall completely in one of the energy bins, we club three energy bins simultaneously to cover the full energy peak. The events under the calculated histogram corresponding to the energy range from 122.5–250 keV accounts for singly and multiply scattered radiations (having energy

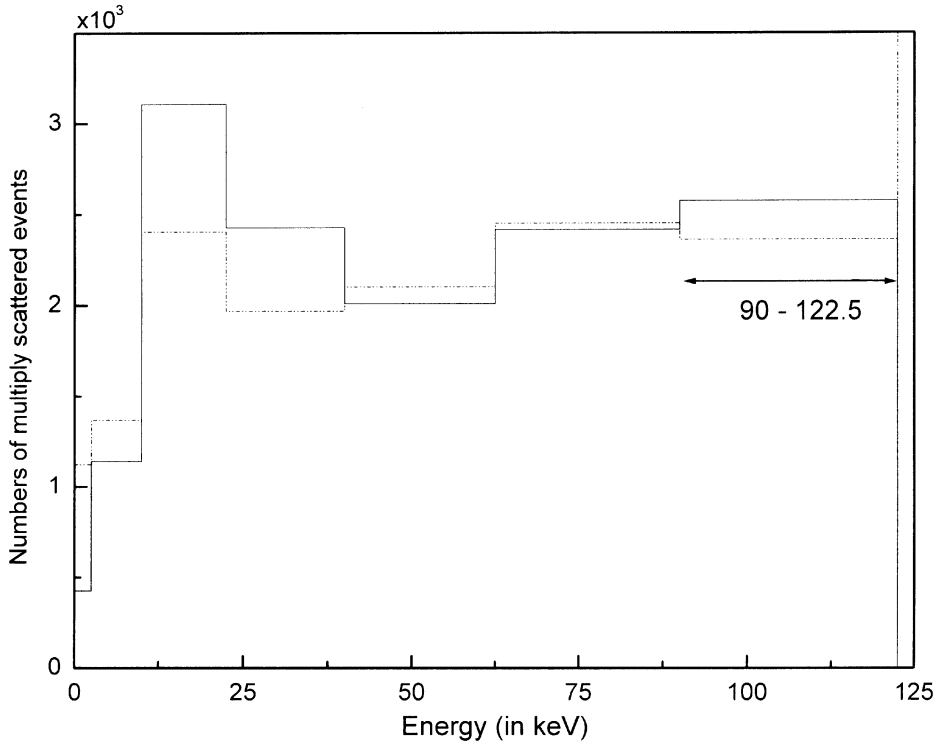

Figure 4. A histogram to evaluate emergent flux from the target corresponding to lower bin mesh of 90–122.5 keV energy.

equal to that of singly scattered ones). The events under Curve b of figure 3 are divided by peak-to-total ratio, $\varepsilon_{\mathrm{p}}(E)$, of the gamma detector and their subtraction from the events under the calculated histogram (Curve c) in the specified energy range results in events not originating from single Compton scattering but having the same energy as in single Compton scattering. These events, when corrected for the intrinsic (crystal) efficiency of the scintillation crystal [11], iodine escape peak [13], and absorptions in the Al-window [14] of the detector and in air [15] present between the target and detector, provide the emergent flux from the target under study at 90° having energy in the range of the inelastically scattered peak.

The bin mesh of energy window 90–122.5 keV (Curve c of figure 3, and dotted curve of figure 4), to the left of the observed inelastic peak accounts for events originating from multiple scatterings and bremsstrahlung produced by recoiling electrons in the thick target. These events do not result from single Compton scattering of 279 keV incident photons. Some of the photons of this energy region get registered in the lower bin meshes owing to partial absorption of energy in the gamma detector. The solid curve of figure 5 is the resulting calculated histogram of $N(E)$ in units of photons corresponding to peak energy bin mesh of 90–122.5 keV. The area of the histogram in this bin mesh divided by intrinsic efficiency of the gamma detector, and corrected for the effects mentioned in the previous paragraph,

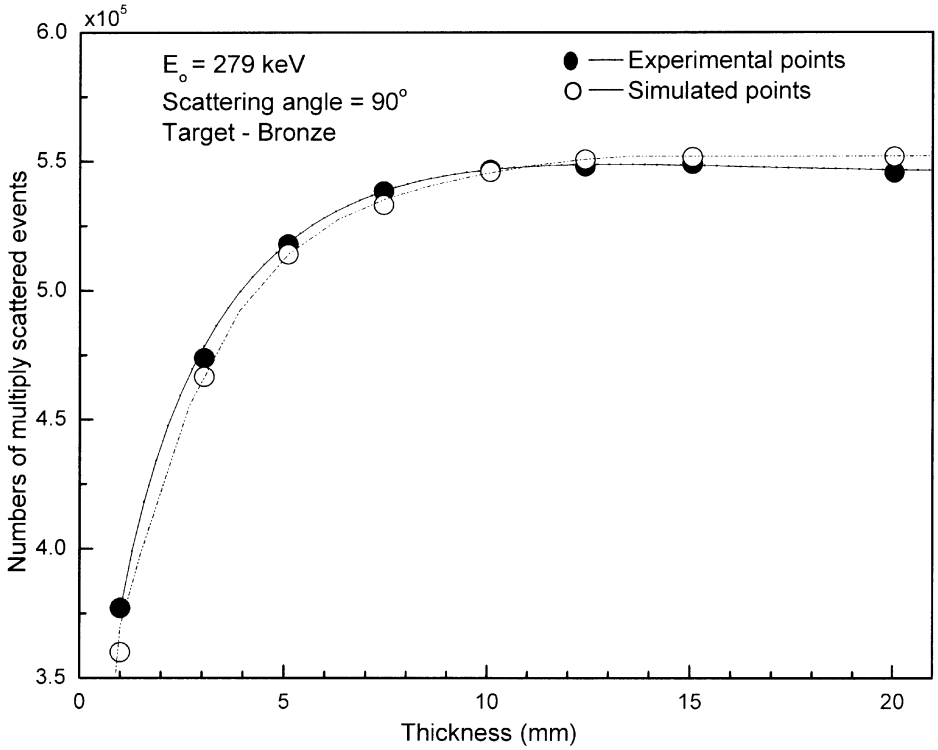

Figure 5. Variations of experimentally observed (solid symbol) and simulated (hollow symbol) numbers of multiply scattered events as a function of target thickness of bronze.

provides the number of photons of this particular energy range emerging from the target in the direction of the detector. This procedure is first applied to the lower bin meshes and is then repeated for different thicknesses of the bronze targets.

The variation of multiply scattered events, having same energy as in singly scattered distribution, is shown in figure 5 as a function of target thickness. The number of multiply scattered events increases with increase in target thickness and then saturates. The increase in the number of multiply scattered photons as thickness increases is caused by an increase in the number of scattering centres. The increase in thickness also results in self-absorption of photons coming out of the target. A stage is reached when thickness of the target becomes sufficient to compensate for the above increase and decrease in the intensity of multiply scattered events. Thus beyond this thickness, the intensity of multiply scattered events does not change with increasing target thickness. The measured value of saturation thickness for 279 keV gamma photons in bronze comes out to be 9.8 mm.

The present experiment is simulated with the Monte Carlo package developed by Bauer and Pattison [16]. The Monte Carlo package has been tested for a number of photons entering the sample and it has been found that there is no appreciable change in the fractional intensity of multiply scattered distribution. The results

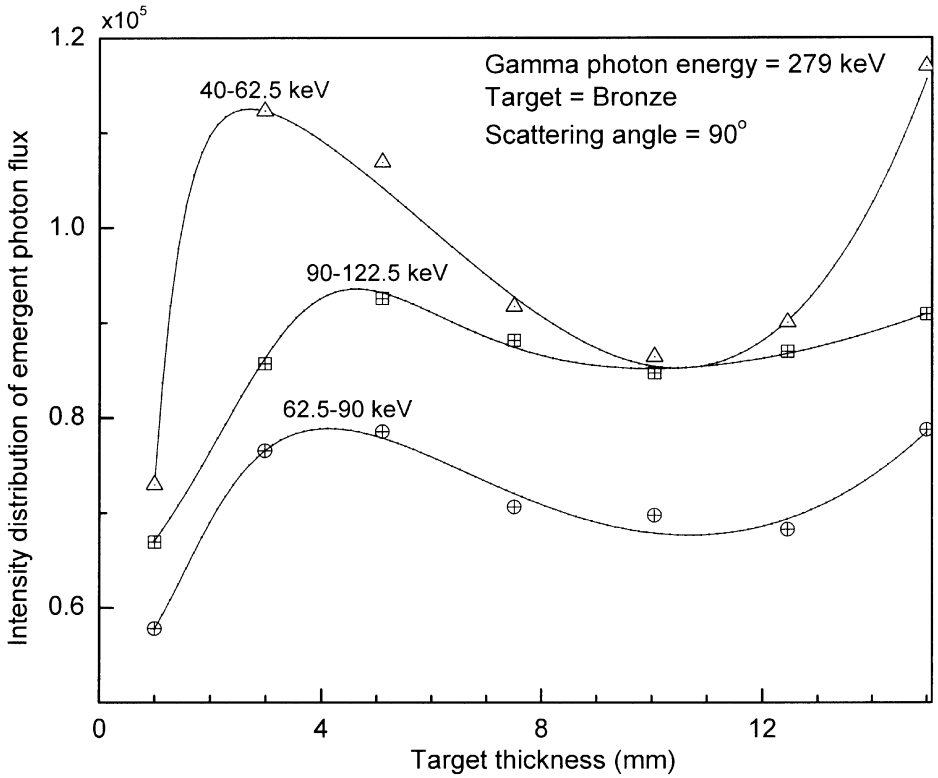

Figure 6. Variation of intensity distribution of emergent photon flux from the targets of bronze in the direction of the gamma detector for the lower bin meshes as a function of target thickness.

based on the Monte Carlo calculations for multiply scattered intensity, at scattering angle of 90° for 279 keV incident gamma photons in our geometrical set-up, are also given in figure 5. The dotted curve is the best-fitted curve corresponding to the simulated data (hollow symbols). The simulated data of multiply scattered intensity also increases with increase in target thickness and then saturates. This behaviour of simulated data supports the present experimental results.

The variation of intensity distribution of emergent photon flux (originating from multiple scattering of incident gamma photons in the targets of bronze and bremsstrahlung produced by slowing down of recoiling electrons in thick target) in the direction of the gamma detector, for the lower bin meshes, is shown in figure 6 as a function of target thickness. In the absence of bremsstrahlung, the intensity distribution (originating from multiple scattering in the target) is expected to increase with target thickness and then saturates, but increasing target thickness also results in self-absorption of the emergent photon flux of that particular energy within the target. The bremsstrahlung intensity is expected to be negligible for thin targets and increases with target thickness. The curves in figure 6 reflect the above two effects and we see that the emergent photon flux in these bin meshes

Table 3. Measured values of saturation depth (thickness) of emergent photons of different energy bins from bronze for 279 keV incident photons.

Energy bin (in keV)	Saturation thickness in bronze target (mm)
40–62.5	2.7
62.5–90	4.1
90–122.5	4.7
122.5–250	9.8

first increases with target thickness, reaches a maximum followed by a decrease in intensity beyond saturation depth due to self-absorption in the target. The measured values of saturation thickness for different energy bins are given in table 3. The saturation thickness of the emergent flux decreases with decrease in energy. On the other hand, increasing thickness results in more bremsstrahlung produced by recoiling Compton and photoelectrons which have continuous energy distribution. Hence the intensity of emergent photons once again shows an increase for higher target thicknesses.

6. Conclusions

Our present results confirm that for thick targets, there is significant contribution of multiply scattered radiation emerging from the target, having energy equal to that of singly scattered Compton process. The present measurements of multiple scattering of 279 keV incident photons in bronze (an alloy having composition of 60% Cu and 40% Sn) are observed for the first time. The simulated and experimental data show similar behaviour. The saturation of intensity of multiple scattering events, under the full energy peak, beyond a particular thickness supports the work of Paramesh *et al* [2] and our recent work [7,8]. The emergent photon flux in the direction of the gamma detector, for the lower bin meshes, shows a broad maximum. The emergent intensity is expected to saturate at a certain depth, but due to the self-absorption in the target and bremsstrahlung, we see an initial decrease and then an increase after the expected saturation depth. The saturation thickness increases with increase in energy of the chosen bin mesh. There are no data available on saturation thickness for comparison with the present results. The detector response unfolding converting the observed pulse-height distributions to a true photon energy spectrum is quite satisfactory. Here it is also important to note that attempts on this objective have been very rare. So our present findings will serve very good reference for further comparison with experimental data of these processes. The work on multiple scattering is in progress under different geometrical conditions for better understanding of the multiple scattering processes. It is further planned to simulate the future multiple scattering experiments with more commonly used EGS4 (electron gamma ray showers) and Geant4 codes.

References

[1] V Halonen and B Williams, *Phys. Rev.* **B19**, 1990 (1979)
[2] L Paramesh, L Venkataramaiah, K Gopala and H Sanjeevaih, *Nucl. Instrum. Methods* **206**, 327 (1983)
[3] T Pitkanen, D Laundy, R S Holt and M J Cooper, *Nucl. Instrum. Methods* **A251**, 536 (1986)
[4] T Pitkanen, M J Cooper, D Laundy and R S Holt, *Nucl. Instrum. Methods* **A257**, 384 (1987)
[5] Manpreet Singh, Gurvinderjit Singh, B S Sandhu and Bhajan Singh, *Appl. Rad. Isotopes* **64**, 373 (2006)
[6] G Barnea, C E Dick, A Ginzburg, E Navon and S M Seltzer, *NDT&E International* **28**, 155 (1995)
[7] Gurvinderjit Singh, Manpreet Singh, Bhajan Singh and B S Sandhu, *Nucl. Instrum. Methods* **B251**, 73 (2006)
[8] Manpreet Singh, Gurvinderjit Singh, Bhajan Singh and B S Sandhu, *Phys. Rev.* **A74**, 042714 (2006)
[9] J H Hubbell, *Rev. Sci. Instrum.* **29**, 65 (1958)
[10] J H Hubbell and N E Scofield, IRE transactions of the professional group of nuclear science (1958) NS-5:156
[11] C E Crouthamel, *Applied gamma-ray spectrometry* (Pergamon Press, London, 1960) pp. 202–216, 673
[12] S D Conte and C Boor, *Elementary numerical analysis* (Tata McGraw Hill, New Delhi, 1980) p. 160
[13] P Axel, *Rev. Sci. Instrum.* **25**, 39 (1954)
[14] W J Veigele, *At Data* **5(1)**, 51 (1973)
[15] J H Hubbell, *Radiat. Res.* **70**, 58 (1977)
[16] Gerrit E W Bauer and P Pattison, *Compton scattering experiments at the HMI* (Hahn-Meitner-Institute für Kernforschung, Berlin) HMI-B 364 (1981) pp. 1–106